Isotactic Polypropylene/Carbon Nanotube Composites Prepared by Latex Technology. Thermal Analysis of Carbon Nanotube-Induced Nucleation

Hans E. Miltner,[†] Nadia Grossiord,[§,⊥] Kangbo Lu,[||,⊥] Joachim Loos,[||,⊥] Cor E. Koning,[†,‡,§,⊥] and Bruno Van Mele*[,†]

Physical Chemistry and Polymer Science and Physical and Colloidal Chemistry, Vrije Universiteit Brussel, Pleinlaan 2, B-1050 Brussels, Belgium; Laboratory of Polymer Chemistry, Eindhoven University of Technology, P.O. Box 513, 5600 MB Eindhoven, The Netherlands; Laboratories of Polymer Technology and Materials and Interface Chemistry, Eindhoven University of Technology, P.O. Box 513, 5600 MB Eindhoven, The Netherlands; and Dutch Polymer Institute, P.O. Box 902, 5600 AX Eindhoven, The Netherlands

Received March 23, 2008; Revised Manuscript Received May 16, 2008

ABSTRACT: During nonisothermal crystallization of highly dispersed polypropylene/carbon nanotube (CNT) composites, considerable heterogeneous nucleation is observed to an extent scaling with the CNT surface area. Saturation occurs at higher loadings, reaching a plateau value for the crystallization onset which is 15 °C higher than in the unfilled matrix. Polymorphic behavior does not occur, as revealed from wide-angle X-ray diffraction. Upon subsequent heating, an increase in the melting temperature is observed due to increased crystalline perfection in the presence of CNTs. The complex multiple melting behavior is interpreted in terms of recrystallization phenomena. A study at varying heating and cooling rates reveals that CNTs affect the chain segment mobility of the matrix and largely inhibit recrystallization upon heating. TEM observation of the nanocomposite morphology evidences the occurrence of a transcrystalline layer around the CNTs. A structure model is presented, in which individually dispersed CNTs are separated from a bulklike polymer phase by a highly ordered crystalline interface with reduced polymer mobility.

1. Introduction

Since their discovery in 1991,[1] carbon nanotubes (CNTs) have emerged as a new class of nanosized filler particles for incorporation into various polymer systems, attracting considerable interest from both academia and industry. Owing to the exceptional intrinsic properties of the filler particles,[2] novel materials can be envisaged which exhibit unprecedented property enhancements, moreover at filler loadings much lower than in conventional composite technology.[3] In the field of thermoplastic nanocomposites, reported property enhancements include improved mechanical performance,[4,5] high thermal and electrical conductivity,[6–8] increased crystallization rate,[9–11] and altered rheological behavior.[12,13]

Because of its outstanding properties, low price, and wide applicability, isotactic polypropylene (iPP) is among the most extensively studied thermoplastics, with widespread application in various composite materials. Over the years, iPP has been reinforced with a wide range of fibers (e.g., carbon, glass, Kevlar, PET, PTFE, natural fibers) as well as other fillers (talc, mica, calcium carbonate, etc.), essentially aiming at improving its mechanical performance. However, the emergence of carbon nanotubes as filler particles has paved the way for potential new applications, in fields which so far have required the use of expensive engineering polymers. For instance, a potentially highly important application is the use of nanocomposite films for antistatic purposes and electromagnetic interference (EMI) shielding.[14,15] The requirements to the material are manifold, however, as films need to be thin and transparent, yet mechanically stable and displaying a sufficiently high electrical conductivity. The use of CNTs as filler particles in iPP may provide a way to fulfill these requirements, as their incorporation simultaneously provides mechanical reinforcement as well as electrical conductivity. A prerequisite for the latter, however, is the achievement of an electrically conductive percolating network of filler particles, at low enough loading so as to preserve the material's transparency.[15]

In most recent reports on iPP nanocomposites the melt blending technique was employed to incorporate the high aspect ratio CNTs into the matrix.[9,16–18] This provides a very simple preparation method, while conventional melt compounding and shaping methods can still be easily applied. However, some of the drawbacks associated with melt compounding methods include high energy cost, risk of filler deterioration during processing, and a generally poor dispersion quality.[9] Solution mixing provides an alternative preparation method[19] but requires the use of organic solvents and is limited to relatively small quantities. The present paper reports a novel latex-based method for the incorporation of single-walled and multi-walled carbon nanotubes (SWCNTs and MWCNTs, respectively) into a polypropylene matrix. In addition to being versatile and environmentally friendly, latex technology allows for the achievement of high dispersion qualities. Moreover, it can be easily extended to any matrix polymer synthesized by emulsion polymerization or brought into the form of a latex otherwise.[20] In the present study, it allows for the preparation of high-performance lightweight iPP nanocomposites, while overcoming the drawbacks of conventional processing methods. A potential extension of this method is its use for the preparation of predispersed masterbatches for subsequent incorporation into a commercial iPP matrix by melt blending. This work also aims at investigating the effect of filler specific surface by comparing

* Corresponding author: Fax +32-(0)2-629.32.78; Tel +32-(0)2-629.32.76; e-mail bvmele@vub.ac.be.
[†] Physical Chemistry and Polymer Science, Vrije Universiteit Brussel.
[‡] Physical and Colloidal Chemistry, Vrije Universiteit Brussel.
[§] Laboratory of Polymer Chemistry, Eindhoven University of Technology.
[||] Laboratories of Polymer Technology and Materials and Interface Chemistry, Eindhoven University of Technology.
[⊥] Dutch Polymer Institute.

10.1021/ma800643j CCC: $40.75
Published on Web 07/16/2008

the two types of nanofiller, i.e., SWCNTs and MWCNTs. The difference in external nanotube surface area is anticipated to considerably affect the nanocomposite properties, as previously evidenced in relation to mechanical properties.[21] The present work provides a direct comparison between the achieved performance levels after incorporation of either nanotube type on three additional fronts, i.e., thermal behavior, crystalline morphology,[22] and electrical properties.[23]

It has been long recognized that the addition of fillers significantly affects the crystallization behavior and resulting crystalline morphology of the iPP matrix. Carbon fiber, among others, was found to strongly nucleate the iPP crystallization, resulting in a peculiar crystalline morphology termed *transcrystallinity*.[24–26] This highly oriented columnar morphology, extending over the entire fiber−matrix interface, is considerably different from the spherulitic crystal growth commonly encountered in iPP. It is, however, generally not associated with polymorphism, unless when crystallized from the sheared melt around a pulled fiber.[27] The origin of transcrystallinity has been the subject of intensive research and is still a matter of debate. Its development is associated with the high density of heterogeneously nucleating sites on the fiber surface, restricting crystal growth to the direction perpendicular to the fiber, with the *c*-axis aligned in the fiber direction.[28] However, several additional factors are believed to influence its formation mechanism, such as epitaxial crystal growth based on lattice matching, surface energy and topology of the fiber, flow-induced crystallization, or residual stresses resulting from a mismatch in the thermal expansion coefficients of fiber and matrix.[24] Transcrystallinity has also been encountered in a number of nanocomposite systems. For instance, nylon-6 crystals were reported to grow perpendicular to dispersed clay platelets,[29] whereas carbon nanotubes were found to template the growth of polyethylene crystals in a direction perpendicular to the nanotubes.[30,31] Crystallization from dilute solution was found to induce structures strongly resembling the shish-kebab morphology in polyethylene and nylon-6,6.[32] For iPP nanocomposites, finally, several reports suggested the occurrence of transcrystallinity, however without providing experimental evidence.[10,19,33] Moreover, contradictory findings subsist as to the possible occurrence of polymorphism in iPP nanocomposites containing carbon nanotubes.[18,33]

In the present study we report on the crystallization and melting behavior of well-dispersed iPP nanocomposites prepared by latex technology, with a focus on differences between SWCNTs and MWCNTs. In a crystallization study, we aim at comparing the nucleating action of both types of nanotubes. During subsequent melting, recrystallization phenomena may occur depending on the applied heating rate, the kinetics of which will be discussed in terms of polymer chain segment mobility. Finally, our attention will be devoted to the specific crystalline morphology of iPP in the presence of carbon nanotubes, allowing us to present a simple model for the structure formation in this type of nanocomposites. The specific transcrystalline morphology of iPP/CNT composites in ultrathin films and in bulk will be further investigated in a second paper.[22] Finally, in a third paper, we focus on the electrical properties of the as-prepared nanocomposites, showing that the presented latex method yields highly conductive nanocomposites with an extremely low percolation threshold.[23]

2. Experimental Section

Materials. Both types of CNTs used in this study were prepared by chemical vapor deposition: thin MWCNTs (Nanocyl-3100) from Nanocyl S.A. (Belgium) and HiPCO SWCNTs from Carbon Nanotechnology, Inc. (USA). The CNTs were used as-received after purification by the supplier (impurities <5 wt % in the MWCNTs and in the range 10−15 wt % in the SWCNTs).

The matrix material is a water-based emulsion of maleic anhydride-grafted isotactic polypropylene (iPP-*g*-MA, further denoted as iPP), commercialized by Solvay S.A. (Belgium) under the trade name Priex801. It was designed for antistatic applications and contains additives enhancing the conductivity. According to the supplier, the aqueous emulsion is composed of 25 wt % of iPP-*g*-MA polymer and 7 wt % of anionic surfactant of the oleic acid type, neutralized by an amino alcohol, the remainder being water. The weight-average molar mass of the polymer is in the range M_w = 50 000−60 000 g/mol with 29 wt % of the iPP-*g*-MA below 20 000 g/mol, as determined by GPC in trichlorobenzene using linear polyethylene standards (measured at DSM Resolve, The Netherlands).

Exfoliation of SWCNTs and MWCNTs. Typically, 0.2 wt % of MWCNTs or 0.5 wt % of SWCNTs was mixed with twice the amount of sodium dodecyl sulfate (SDS) in water. The mixture was sonicated at 20 W (Vibracell VC750) until maximum debundling was achieved, as determined by UV−vis spectroscopy.[34,35]

Nanocomposite Preparation. After sonication-driven debundling of carbon nanotubes, the colloidally stable dispersion was directly mixed with the Priex801 emulsion. The mixture was subsequently freeze-dried (Chris Alpha 2-4) and the obtained powder degassed and compression-molded into films (2 min at 170 °C under 100 bar pressure, Collin Press 300G; a short stay in the melt was chosen to avoid thermal stability issues).

Characterization. The crystalline structure of the matrix was assessed from wide-angle X-ray diffraction (WAXD) experiments at room temperature using a Siemens D5000 diffractometer with Cu Kα radiation, operated at an acceleration voltage of 35 kV and a current of 40 mA.

Differential scanning calorimetry (DSC) experiments were performed in either conventional or modulated mode (modulated temperature DSC (MTDSC)) on a helium-purged TA Instruments 2920 DSC with MDSC option and equipped with a refrigerated cooling system (RCS). Temperature and enthalpy calibration were performed using an indium standard. Conventional DSC experiments were performed at 2.5 or 15 °C/min rates, whereas MTDSC measuring conditions were a rate of 2.5 °C/min and an applied temperature modulation of ±0.5 °C/60 s. Sample masses were typically in the range 3−5 mg, contained in nonhermetic aluminum crucibles (Perkin-Elmer).

Rapid-scanning DSC experiments were performed on a novel device known as Project RHC (TA Instruments, New Castle, DE), specifically designed for operation at high scanning rates (up to 2000 °C/min in ballistic infrared heating or liquid nitrogen cooling).[36] Temperature and enthalpy calibration were performed using an indium standard. Experiments in heating were conducted under a nitrogen atmosphere after ballistic cooling under helium purge. Sample pans weighing less than 2 mg were used, with sample masses in the range 0.08−0.23 mg.

For transmission electron microscopy (TEM) characterization, the as-prepared mixture of iPP latex and aqueous MWCNT dispersion was deposited on carbon-coated copper grids. A thermal treatment at 180 °C for 10 min was applied to the sample, after which it was cooled to 50 °C at a rate of 5 °C/min. TEM images were recorded on a Titan-Krios operated at 300 kV acceleration voltage or on a Tecnai G^2 20 operated at 200 kV (both Fei Co., The Netherlands).

3. Results and Discussion

CNTs are well-known to impart profound changes to the crystallization behavior of semicrystalline polymers. Not only do they affect the crystalline morphology, generally promoting a fibrillar rather than a spherulitic structure,[37] they also strongly modify the kinetics of the crystallization process as a result of their nucleating action.[11,38] Furthermore, CNTs may induce polymorphism in certain systems, promoting crystallization into

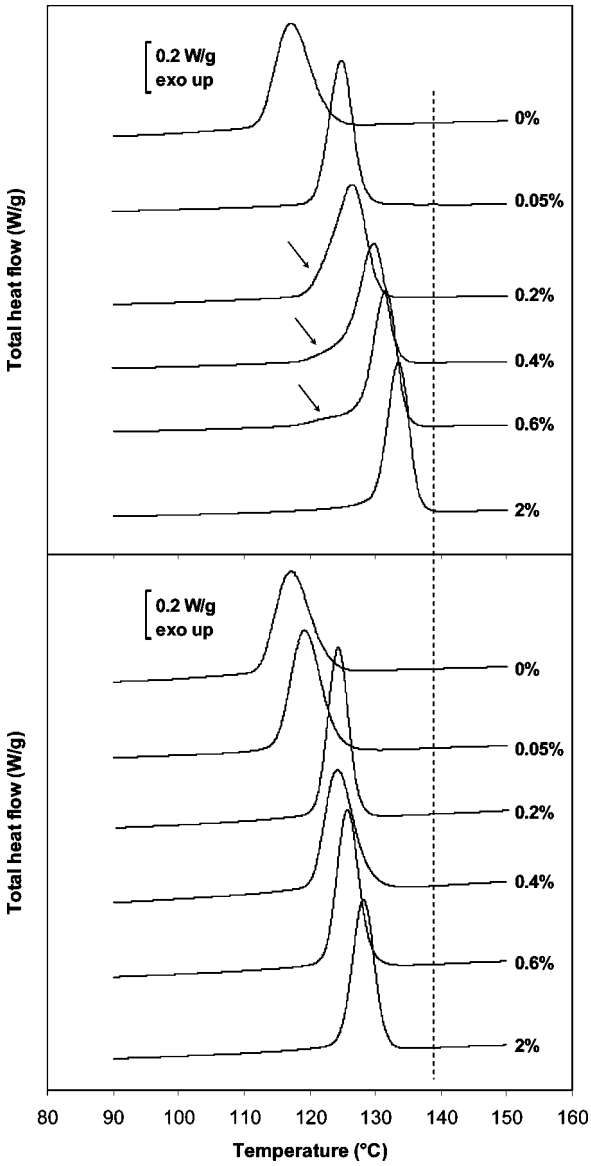

Figure 1. MTDSC cooling traces at 2.5 °C/min for iPP nanocomposites containing SWCNTs (top) and MWCNTs (bottom). The vertical dashed line marks the highest achieved onset temperature of crystallization; CNT loadings are indicated in wt %; for arrows: see explanation in text.

specific crystal forms other than those encountered in the unfilled materials.[39,40]

In this work, the thermal properties of well-dispersed iPP nanocomposites are investigated. The high dispersion quality achieved by the employed latex-based approach was demonstrated elsewhere;[20,22,23] it is illustrated, for the present iPP nanocomposites, by the extremely low percolation thresholds of 0.1 and 0.05 wt % filler loading in case of MWCNTs and SWCNTs, respectively.[23] A detailed calorimetric analysis of the crystallization and melting behavior is conducted by both conventional DSC and MTDSC, aiming at assessing the changes in the thermal behavior of the matrix, induced by the presence of either SWCNTs or MWCNTs. Results from thermal analysis are complemented by morphological analysis.

3.1. Nucleating Ability of Carbon Nanotubes. Nonisothermal crystallization experiments have been conducted by MTDSC on both SWCNT- and MWCNT-based nanocomposites (Figure 1). An upward shift in the crystallization onset and peak temperatures can be observed in both cases, even at CNT loadings as low as 0.05 wt %, suggesting a high degree of crystal

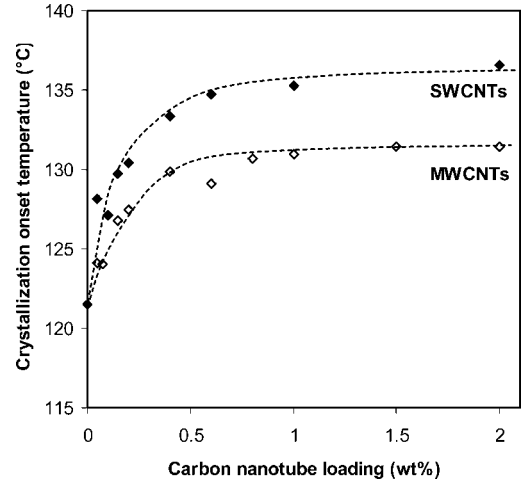

Figure 2. Crystallization onset temperatures from nonisothermal crystallization experiments at 2.5 °C/min plotted as a function of CNT loading.

nucleation on the surface of the CNTs. The overall crystallization process is accelerated as a result of the presence of filler particles, providing a tremendous amount of sites for heterogeneous nucleation and increasing the onset temperature of crystallization with respect to the homogeneously nucleated unfilled iPP. However, changes in the developed degree of crystallinity could not be observed based on a comparison between the recorded crystallization enthalpies for all samples.

When comparing the nucleating ability of SWCNTs and MWCNTs, it appears that the effect of SWCNTs is more pronounced. This is visualized by the vertical dashed line in Figure 1, marking the onset of crystallization at 2 wt % SWCNT loading, which is roughly 15 °C higher than in unfilled iPP and ca. 5 °C higher than with MWCNTs at equal loading. In addition, considerable narrowing of the crystallization peak occurs with increasing filler loading along with an increased intensity of the signal, suggesting a progressive increase in the overall crystallization rate. At intermediate SWCNT loadings of 0.2−0.4 wt %, a weak shoulder can be observed at the low-temperature side of the crystallization exotherm (see arrows in upper part of Figure 1), which is not observed in case of MWCNTs. The occurrence of such shoulder might suggest that, whereas a large portion of the matrix material undergoes considerable crystal nucleation, part of it remains less affected. This effect disappears upon further increasing the SWCNT loading, suggesting that at higher loadings the complete matrix is being effectively nucleated.

Figure 2 provides a direct comparison of the nucleating action of both types of CNTs in iPP. The onset temperature of crystallization is increased for both types of CNTs. Interestingly, however, the effect is considerably more pronounced in the case of SWCNTs, which already exhibit strong nucleation at extremely low filler loadings. A similar nucleation effect with MWCNTs requires 2−4 times higher loading. Figure 2 also shows that the upward shift in the crystallization onset temperature levels off at a plateau value, evidently suggesting saturation of the nucleating effect. The attained plateau value is considerably higher in the case of SWCNTs, exceeding that of MWCNT-based nanocomposites by more than 5 °C.

The observed differences in the crystallization behavior of these systems, both with respect to the dependence on nanotube loading as well as relating to the plateau value of the crystallization onset, result from the large discrepancy in the specific surfaces of both types of CNTs. If D_{CNT} and ρ_{CNT} denote the CNT diameter and density, respectively, it is readily demon-

strated that, for a given mass fraction, the outer surfaces S provided by the two types of CNTs relate as

$$\frac{S^{\text{SWCNTs}}}{S^{\text{MWCNTs}}} = \frac{\rho_{\text{MWCNT}} D_{\text{MWCNT}}}{\rho_{\text{SWCNT}} D_{\text{SWCNT}}}$$

For the CNTs used in this work, values of $\rho_{\text{MWCNT}} = 2150$ kg/m^3, $\rho_{\text{SWCNT}} = 1500$ kg/m^3, $D_{\text{MWCNT}} = 14$ nm, and $D_{\text{SWCNT}} = 9$ nm have been reported.[21] Taking these values into account, the above ratio of external surfaces equals 2.2, showing that at equal mass fraction SWCNTs provide more than twice as much surface as MWCNTs. Note, in addition, that the above value of $D_{\text{SWCNT}} = 9$ nm was reported as an estimation for the average diameter of bundles of SWCNTs, since perfect exfoliation into individual SWCNTs could not be achieved by the employed solution mixing method.[21] The present surfactant-assisted latex exfoliation method, however, does provide a much more efficient SWCNT dispersion, increasing the above ratio of external surfaces to a factor 20 for $D_{\text{SWCNT}} = 1$ nm, i.e., for individually dispersed SWCNTs. In other words, at equal mass fraction in CNTs, i.e., at ca. 1.4 times higher volume fraction, SWCNTs provide 20 times the external surface of MWCNTs under perfect exfoliation conditions. In light of these facts, the results shown in Figure 2 suggest that the nucleation ability is directly related to the effective surface area provided by the carbonaceous filler. These results also confirm earlier results comparing the effect of various types of MWCNTs and carbon nanofibers on the crystallization of nylon-12.[11]

The fact that the crystallization onsets level off at higher filler loadings and finally attain a plateau value is indicative of some degree of nucleation saturation. An incomplete CNT exfoliation at higher loadings provides a possible explanation, as worse nanofiller dispersion at higher mass (or volume) fractions implies that much of the outer surface of the nanotubes becomes inaccessible for crystal nucleation. Incomplete exfoliation of CNT bundles due to van der Waals interactions and—especially in the case of MWCNTs—nanotube entanglement might well explain part of the nucleation saturation observed. An alternative explanation may imply that, from a certain loading onward, the crystallization rate levels off as a result of the fact that crystal growth becomes the rate-determining factor.[30] Further increasing the loading does effectively increase the nuclei density, but under the resulting time and temperature conditions crystallization proceeds more slowly, resulting in a leveling off of the crystallization onset. The rate-determining factors can either be the high crystallization temperature, resulting from the nucleating action and diminishing the thermodynamic driving force for crystallization, or limitations in the diffusion of polymer chains toward the growing crystal front. The latter might result from reduced polymer mobility and from chain diffusion constraints in a geometrically confined space, as the average interparticle distance is severely reduced at higher loadings. Still, none of these factors can explain the fact that different plateau levels of the crystallization onset are obtained for SWCNT- and MWCNT-based nanocomposites, since both higher crystallization temperature (ca. 5 °C higher) and smaller average intertube distance (roughly a factor 2−15 lower) would make SWCNTs less favorable from this point of view. Even though rate-determining factors may as well play a role, an explanation in terms of incomplete CNT exfoliation is therefore more likely.

With respect to the above discussion on the crystallization of the iPP matrix, it is worth noting that the nucleating action of SWCNTs, increasing the crystallization onset and peak temperatures by ca. 15 °C, is comparable to that of conventional nucleating agents. Indeed, shifts of up to 15−17 °C have been reported after incorporation of sorbitol derivatives or sodium benzoate into iPP.[41,42] Moreover, saturation of the nucleating effect was equally observed for such conventionally nucleated

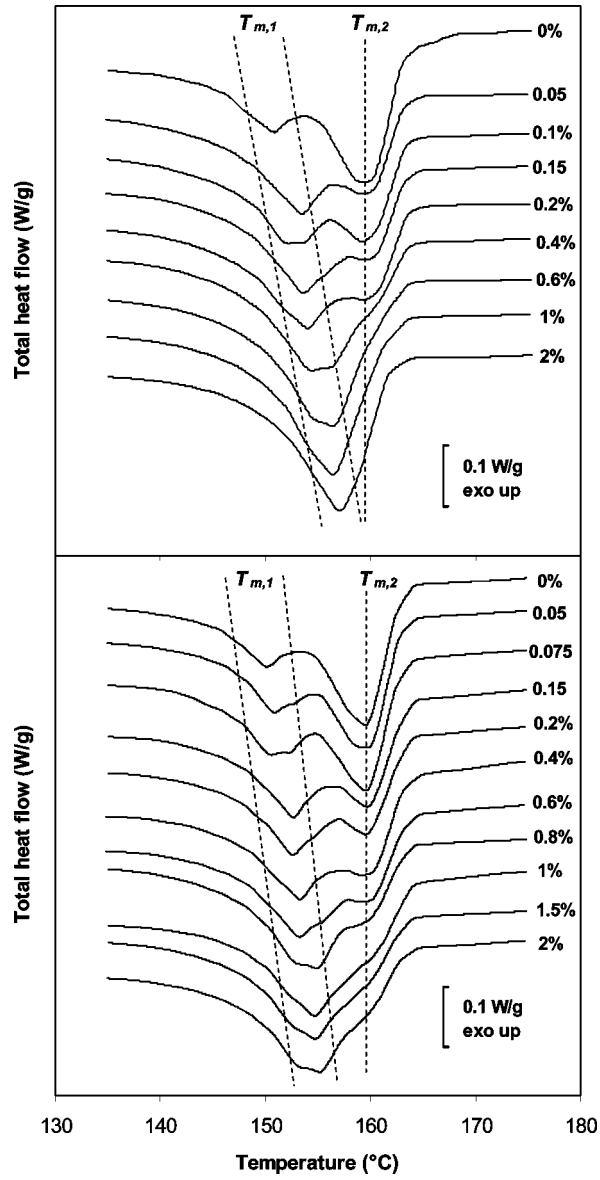

Figure 3. MTDSC total heat flow traces during heating at 2.5 °C/min of iPP nanocomposites containing SWCNTs (top) and MWCNTs (bottom). The dashed lines are guidelines to the eye showing the position of the melting peaks for the different systems ($T_{m,1}$ marked as a broad melting region and $T_{m,2}$ as a single peak).

systems and was attributed to agglomeration of the nucleating particles due to overdosage, limiting the number of effective nuclei to ca. $10^{12}-10^{13}$/cm^3.[41] It is striking that the number of SWCNTs or MWCNTs present in the iPP samples in the considered loading range amounts to the same order of magnitude. This suggests that the CNTs, especially the SWCNTs, are equally effective nucleating agents as the more conventional ones, even though the nucleating action can be potentially limited by their incomplete exfoliation.

3.2. Melting Behavior of iPP Nanocomposites. The melting behavior after nonisothermal crystallization was investigated by MTDSC at a heating rate of 2.5 °C/min. Figure 3 shows the melting traces for the iPP nanocomposites containing SWCNTs (top) or MWCNTs (bottom). Note that similar melting traces are obtained from conventional DSC experiments; effects related to the presence of an imposed temperature modulation can therefore be excluded. Clearly, the presence of CNTs has a dramatic impact on the melting behavior of the matrix material. Whereas the unfilled matrix unambiguously shows double

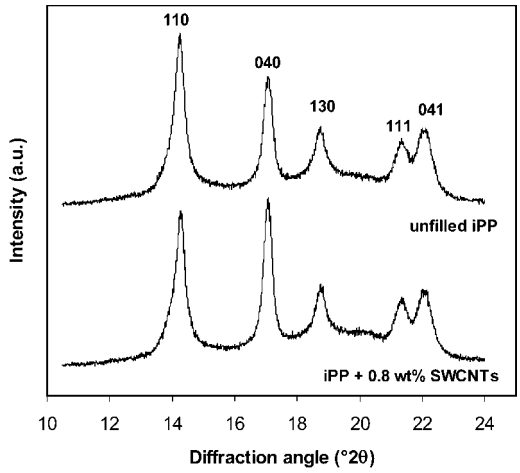

Figure 4. WAXD profiles for unfilled iPP (top) and for a nanocomposite containing 0.8 wt % of SWCNTs (bottom), showing the characteristic diffraction peaks of α-crystalline iPP.

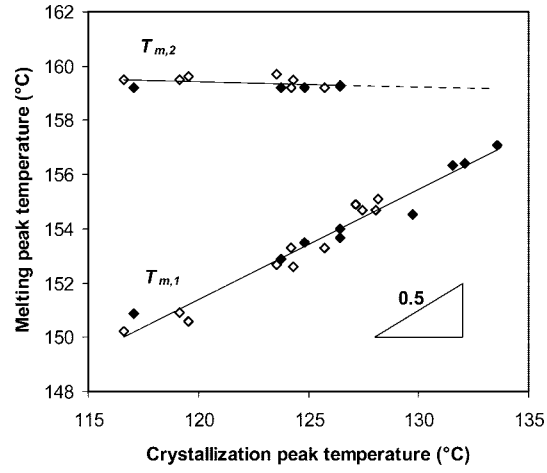

Figure 5. Melting peak temperatures $T_{m,1}$ and $T_{m,2}$ plotted against crystallization peak temperature for iPP filled with various loadings of SWCNTs (closed symbols) or MWCNTs (open symbols). Crystallization and melting peak temperatures were obtained from nonisothermal MTDSC experiments and straight lines from linear regression.

melting behavior, the shape of the melting transition progressively evolves toward single melting with increasing SWCNT content. Indeed, the lower melting peak $T_{m,1}$ progressively shifts to higher temperature upon increasing the filler loading, until it finally almost coincides with the higher melting peak $T_{m,2}$ at 2 wt % SWCNT loading. Even though an upward shift in $T_{m,1}$ can also be observed for MWCNT composites, the effect is less pronounced than in the case of SWCNTs, with double melting behavior prevailing even at higher loading.

Multiple melting behavior is generally assumed to result from polymorphism, from the successive melting of crystal populations with distinct degrees of perfection, or from the rapid succession of melting−crystallization−melting or reorganization phenomena. The impact of fillers on the polymorphic behavior of iPP has been extensively reported over the years.[43] Some authors reported that CNTs as well can induce crystallization of iPP in the hexagonal β-polymorph instead of the more common monoclinic α-form.[33] Since both polymorphs display distinct melting temperatures,[43] the observed changes in the shape of the melting transition in the presence of CNTs might potentially be the result of an altered balance between crystal forms simultaneously present in the sample.

Figure 4 shows the WAXD profiles at room temperature for the unfilled matrix and for a nanocomposite containing 0.8 wt % SWCNTs. In both cases the typical pattern of α-crystalline iPP is found, with no indication of β-phase iPP.[28] It can therefore be concluded that CNTs have a strong α-nucleating effect on iPP and that the complex melting transition of the nanocomposites originates from the fusion of polymer crystals with varying lamellar thicknesses, either simultaneously present or as a result of recrystallization phenomena. Note that such multiple melting behavior has been previously attributed to the β-nucleating action of chemically modified CNTs, however, without providing essential evidence from WAXD experiments.[33]

According to classical polymer crystallization theory,[44,45] the melting temperature of a crystal, T_m, is determined by its lamellar thickness. The latter, on the other hand, is inversely proportional to the supercooling below the equilibrium melting point T_m^∞. An equation relating the observed melting temperature to the crystallization temperature could therefore be proposed and led to the well-known linear Hoffman−Weeks method, by which the equilibrium melting temperature is commonly determined as the intersection of two straight lines:[45] the experimentally recorded T_m plotted against T_c (with a slope slightly below $^1/_2$ in most cases) and the line $T_m = T_c$ (slope 1). This diagram is imperatively constructed for isothermally crystallized samples, but the strong nucleation in the presence of CNTs allows a similar diagram to be constructed for nonisothermally crystallized samples, as shown in Figure 5, providing information on the complex melting behavior of the investigated nanocomposites. To this end, the lower melting peak temperature $T_{m,1}$ and the higher melting peak temperature $T_{m,2}$ are plotted as a function of the corresponding crystallization peak temperature (Figure 5). With respect to the lower melting peak, it appears that both SWCNT- and MWCNT-based systems follow the same experimentally recorded $T_{m,1}-T_c$ relationship, with a slope close to $^1/_2$. Note also that extrapolation yields a T_m value of 173 °C, which is only slightly lower than the T_m^∞ values commonly reported in the literature for neat iPP,[46] in accordance with the presence of grafted maleic anhydride moieties in this particular iPP grade.[47] These data therefore clearly obey a T_m vs T_c relationship as expected from a linear Hoffman−Weeks plot, demonstrating that the progressive increase in the melting temperature $T_{m,1}$ upon increasing the CNT content (Figure 3) results from an increased lamellar thickness. We assume that this is a direct consequence of the nucleating action of the CNTs, resulting in polymer crystals being formed at a higher temperature in a nonisothermal experiment, consequently displaying an increased lamellar thickness. This assumption is supported by a recent report, in which SAXS was employed for characterizing the crystalline structure in iPP nanocomposites after nonisothermal crystallization.[19] Note that equal melting temperatures are observed for iPP and iPP/CNT samples *isothermally* crystallized at equal supercooling (not shown).

Figure 5 also shows a T_m vs T_c representation for the higher melting peak $T_{m,2}$, as far as an individual high melting peak could be discerned, and its linear extrapolation for those samples displaying a shoulder at the high temperature end of the melting transition. Interestingly, $T_{m,2}$ appears to be independent of the crystallization temperature during cooling, suggesting that the high melting peak corresponds to a crystalline fraction formed upon heating of the samples, with invariable lamellar thickness. MTDSC was therefore used to investigate the occurrence of recrystallization/reorganization phenomena in unfilled iPP and in the nanocomposite samples.

3.3. MTDSC Study of Recrystallization during Complex Melting. In polymers nonisothermally crystallized from the melt, the observed crystalline lamellar thickness generally displays a rather broad distribution due to the different levels of supercool-

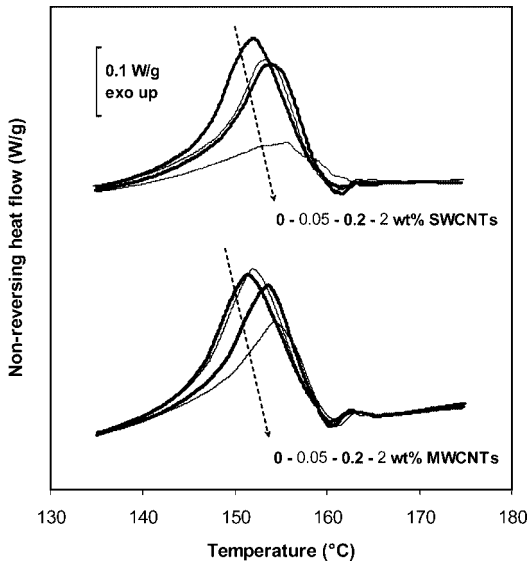

Figure 6. MTDSC nonreversing heat flow traces recorded during heating runs at 2.5 °C/min through the melting region for iPP nanocomposites containing indicated loadings of SWCNTs (top) and MWCNTs (bottom).

ing at which crystals were formed. Moreover, secondary crystals with a lower degree of perfection occur in between the primary lamellae. Broad melting transitions are therefore generally observed, reflecting the wide range of crystal populations simultaneously present in the sample. Accordingly, the apparent discretization in the shape of the lower melting peak ($T_{m,1}$, Figure 3) might reflect the occurrence of different lamellar thicknesses, resulting from specific crystalline morphologies simultaneously present in the sample. When heated slowly through their melting region, however, less stable crystallites may melt and reattach at the edges of the more perfect crystalline lamellae still present in the sample. The crystalline lamellar thickness has been shown to increase upon recrystallization, attesting for increased crystalline perfection and resulting in higher melting temperatures for that crystalline fraction.[48,49] Note that an alternative mechanism of crystalline perfectioning has also been reported, which occurs without preceding partial melting. In that case, a progressive and continuous increase in crystalline lamellar thickness is observed upon heating by in-situ SAXS analysis, however without noticeable effect in the calorimetric signals during the heating run. In this case the mechanism is referred to as reorganization rather than recrystallization.[49]

As in other polymers, recrystallization phenomena are commonly observed in iPP heated slowly through the melting region. This often results in a rather complex shape of the melting transition, generally involving multiple melting peaks.[50,51] In that sense, the complicated melting behavior shown in Figure 3 suggests the occurrence of recrystallization phenomena during the slow heating experiments. MTDSC allows for a more detailed study of possible recrystallization phenomena: melting generally occurs in both the nonreversing and the reversing heat flow signals, whereas crystallization is most often restrained to the nonreversing signal.[52] The total heat flow signal depicted in Figure 3 therefore only provides part of the information.

Figure 6 shows the nonreversing heat flow signals in the melting region of the unfilled iPP as well as for a number of SWCNT and MWCNT composites. Clearly, the nonreversing heat flow signals of all samples contain a predominantly exothermic contribution, attesting to the occurrence of recrystallization phenomena. The double melting behavior displayed in the total heat flow signal (Figure 3) therefore unambiguously originates from the succession of melting of a crystalline fraction of lesser perfection, intermediate recrystallization, and finally melting of a perfectioned crystal population. This mechanism also provides an explanation for the relationship displayed by $T_{m,2}$ in the T_m vs T_c plot of Figure 5. Whereas $T_{m,1}$ shows a progressive increase with increasing CNT loading, resulting from their nucleating action which affects the supercooling at the crystallization temperature, $T_{m,2}$ remains virtually constant, irrespective of the CNT content. This high melting peak therefore corresponds to the fusion of a perfectioned crystalline fraction of invariable lamellar thickness, which for all samples was formed at equal supercooling during heating.

Interestingly, Figure 6 also reveals that, with increasing CNT loading, the onset of the recrystallization phenomenon is progressively shifted to higher temperature, along with a progressive decrease in the enthalpy of the exothermic contribution. This indicates that the recrystallization phenomenon is progressively suppressed in the presence of an increasing loading of CNTs.[19] This effect is even more pronounced for SWCNTs as compared to MWCNTs at equal loading, and it is the origin of the changing balance in the relative importance of both melting peaks in Figure 3 as a function of increasing loading. It again demonstrates that SWCNTs have a larger influence on the iPP matrix than MWCNTs, not only more strongly nucleating its crystallization but also more strongly affecting the subsequent melting behavior.

It is tempting to relate the suppression of the recrystallization phenomenon to the nature of the crystalline phase formed during cooling. As previously discussed, the progressive increase in $T_{m,1}$ points at an increasing degree of crystalline perfection. It was argued that this is due to the higher crystallization temperature during cooling because of the nucleating action of the CNTs. A straightforward conclusion is therefore that the recrystallization phenomenon does not occur to such high extent in the presence of CNTs, simply because the amount of less perfect crystals present in the sample is much lower. Still, the endset temperature of melting, corresponding to the fusion of the most perfect crystals present, is the same in all samples, filled or not (Figure 3). Thus, it appears that recrystallization only sets in at higher temperature in the filled samples because of the higher initial degree of crystalline perfection, finally resulting—in all samples—in the presence of a crystalline fraction of highest possible perfection under the conditions applied.

Although satisfying at first sight, this explanation does not account, however, for the fact that the fraction of highly perfectioned crystals remains much lower in the samples filled with CNTs, even though the unchanged endset temperatures suggests that crystal perfectioning is possible and to some extent does occur in all samples investigated. A series of experiments with varying cooling and heating rates was therefore conducted in order to further address this issue.

3.4. Effect of Cooling and Heating Rates on Recrystallization Phenomena. Since recrystallization essentially concerns the least perfect crystals present in the polymer, it is anticipated that these phenomena can be accentuated by applying higher cooling rates during nonisothermal crystallization of the sample. On the other hand, recrystallization requires time to occur, and increasing the heating rate when scanning through the melting transition is therefore a way to avoid these phenomena.[50] Modifying the experimental time scale, i.e., the scan rate in a DSC experiment, may as such provide information on the characteristic time scale of the kinetic process involved, as illustrated in Figure 7.

The effect of increasing the cooling rate can be observed when comparing traces A and B in Figure 7, both recorded at a low heating rate of 2.5 °C/min. With a higher cooling rate during the preceding nonisothermal crystallization, the recrystallization

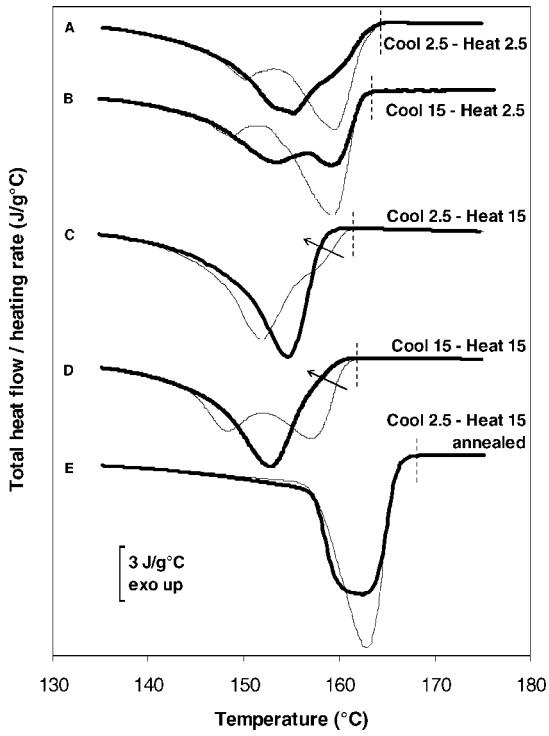

Figure 7. (MT)DSC heating traces in the melting region of unfilled iPP (thin lines) and a nanocomposite containing 2 wt % of MWCNTs (thick lines). The cooling and heating rates are indicated in °C/min (slow heating from MTDSC, fast heating from conventional DSC); heat flows normalized for varying heating rates; vertical dashed lines denote the endset temperatures of melting (see discussion in text).

phenomenon gains importance in both the unfilled iPP and the nanocomposite. The altered balance between the lower and higher melting peaks clearly evidences a changing degree of crystalline perfection, induced by the different thermal treatments. Note also that the endset temperature of melting is somewhat decreased for the rapidly cooled samples, indicating that they retain a slightly lower degree of crystalline perfection despite obvious recrystallization during slow heating.

At equal cooling rate, on the other hand, the effect of increasing the heating rate can be evaluated by comparing traces A and C. For the unfilled sample, recrystallization during fast heating is largely suppressed, as opposed to the situation under slow heating conditions. For the MWCNT-filled sample, recrystallization even no longer seems to occur, resulting in a lower endset temperature of melting as marked by the arrow in Figure 7, traces C. Unlike under slow heating conditions, this result suggests that the final degree of crystalline perfection remains lower in the nanocomposite sample than in the unfilled material, an effect even more accentuated for the rapidly cooled samples in trace D. Prominent double melting behavior is observed in the unfilled sample, showing that the degree of crystalline perfection after the cooling run is lower than in the slowly cooled sample (trace C). The filled sample, however, still exhibits single melting behavior, despite the much lower crystalline perfection, with only a slight shoulder attesting for recrystallization. Hence, the observed differences in the melting endset temperatures of filled and unfilled iPP under fast heating conditions, as marked by arrows in Figure 7, convincingly show that the diminished recrystallization is not only related to the higher initial crystalline perfection in the presence of CNTs. In addition to the latter effect, a partial or even complete suppression of the recrystallization phenomenon occurs in the presence of CNTs, which becomes particularly noticeable under kinetically unfavorable fast heating conditions, pointing at a reduced mobility of the polymer chain segments in the presence of filler particles. However, when sufficient time is given to allow for crystallite melting, reorganization, and subsequent recrystallization at an existing crystalline lamella, the degree of crystal perfection can attain a level comparable to that in unfilled iPP. This is the case under slow heating conditions but is even more pronounced after an isothermal annealing step, where time scale issues become fully irrelevant (30 min at 152 °C). After annealing, the exact same endset temperature of melting is found for the filled and unfilled samples, even at a high heating rate of 15 °C/min (trace E as compared to trace C). It moreover clearly exceeds the endset values from all other traces in Figure 7, showing that a higher degree of crystal perfection is attained after annealing.

Potentially important factors capable of kinetically suppressing the recrystallization phenomena under the conditions chosen are the occurrence of polymer−filler interactions, increases in viscosity, and effects related to geometrical confinement. Even though van der Waals interactions between iPP and CNTs are rather weak, they may affect the polymer crystallization since this is known to be extremely sensitive to subtle changes in the chain segment mobility, as was recently demonstrated by a novel methodology based on quasi-isothermal crystallization.[53–55] Therefore, even the weakest of interactions might be reflected in changes in the recrystallization behavior, especially in view of the tremendous interfacial area provided by the nanofiller. Viscosity increases related to the formation of a percolating network of filler particles might equally affect the recrystallization behavior, as the impeded segmental motion of the polymer[13,56,57] may imply a reduction in the rate of polymer chain reorganization at the crystal−melt interface. Finally, geometrical confinement needs to be considered as the average distance between well-dispersed filler particles becomes much smaller than the typical radius of gyration of the unperturbed polymer,[4] hence also influencing its local segmental mobility and potentially hampering recrystallization phenomena.

In any case, irrespective of the mechanism responsible for the suppressed recrystallization, SWCNTs are anticipated to display a much more pronounced effect than their multi-walled counterparts. This was already noticed with respect to the nucleating action of the fillers as well as in relation to their effect on the melting behavior of the matrix polymer. A key reason for their accentuated influence on the polymer in the considered nanocomposites is the much higher surface area they provide at equal mass fraction. Consequently, SWCNTs are also believed to more strongly affect the recrystallization behavior of iPP upon heating, as experimentally confirmed at low heating rates in Figure 8 (compare traces A and B). For higher heating rates, as in traces C and D, recrystallization is completely suppressed in the presence of SWCNTs, resulting in a lower endset of melting as compared to unfilled iPP. In the MWCNT-filled system a slight shoulder at the high temperature end of the transition still accounts for some extent of recrystallization, but the crystalline perfection still does not reach that obtained in the unfilled material.

Further confirmation of the suppressed recrystallization in SWCNT nanocomposites was obtained from *rapid-scanning DSC* experiments at varying heating rates (Figure 9). After ballistic cooling, unfilled iPP shows clear double melting behavior for heating rates up to 100 °C/min. Moreover, a slight shoulder at the high temperature end of the melting transition indicates that some extent of recrystallization even persists up to heating rates as high as 250 °C/min; it is only fully suppressed at a heating rate of 500 °C/min. In sharp contrast, iPP filled with 2 wt % of SWCNTs shows single melting behavior at all heating rates (apart from a possible weak shoulder at 20 °C/min), demonstrating that recrystallization phenomena are effectively suppressed. For the first time, these observations

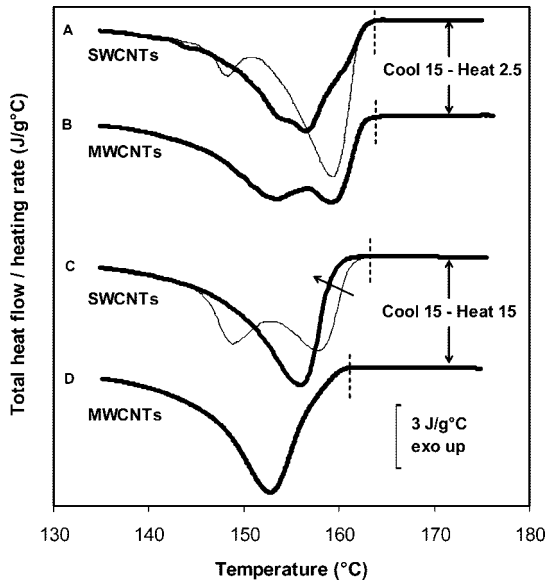

Figure 8. (MT)DSC heating traces in the melting region of unfilled iPP (thin lines) and nanocomposites containing 2 wt % of MWCNTs or SWCNTs (thick lines, as indicated). Measuring conditions and data analysis as in Figure 7.

therefore unambiguously evidence some degree of kinetic hindrance in CNT-filled iPP systems, as a result of alterations in the local mobility of the matrix polymer, induced by the vicinity of the filler particles. On the basis of the observation of an altered crystallization, melting, and recrystallization behavior, it is also anticipated that the presence of nanofiller particles affects the local morphology of the matrix polymer, resulting in a very specific crystalline microstructure characteristic for the considered nanocomposite materials.

3.5. Crystalline Morphology and Structure Model. *Transcrystalline Morphology.* In view of the remarkable changes in the crystallization and melting behavior of iPP nanocomposites, as highlighted in the above discussion, a modification in the crystalline morphology of the matrix polymer can be anticipated.

Figure 10 shows a bright-field TEM micrograph of an ultrathin iPP/MWCNT composite film. The sample was first kept isothermally in the melt at 180 °C for 10 min and subsequently cooled down to 50 °C at a cooling rate of 5 °C/min to resemble the nonisothermal crystallization conditions used for the above (MT)DSC analysis. The top left part of the image shows a complex crystalline morphology with individual crystalline lamellae extending in various directions without apparent preferential orientation. This situation corresponds to the spherulitic crystalline morphology generally obtained in bulk iPP. In the right part of Figure 10, however, an individual MWCNT can be clearly discerned, surrounded over its complete length by crystalline lamellae growing perpendicular to the CNT surface. Note that the orientation of the individual crystalline lamellae is even adjusted to match the curvature of the MWCNT. This image convincingly demonstrates the occurrence of a transcrystalline layer around the CNTs, resulting from the high nucleating efficiency of their surface and the high nucleation density supplied. It also provides the first experimental evidence for transcrystallization on individual CNTs in iPP nanocomposite systems, the occurrence of which had been suggested in a number of earlier reports[10,18,33] and was very recently demonstrated for fibers of aggregated CNTs.[58] The issue of transcrystallinity has also been addressed for nanocomposite systems based on nylon-6,[29] polyethylene,[30,31] or poly(vinyl alcohol),[21] showing that it might well concern a general

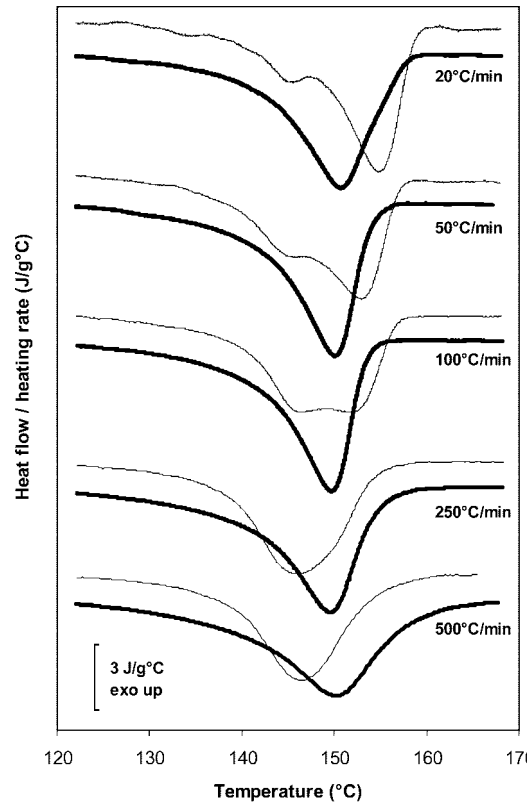

Figure 9. Rapid-scanning DSC heating traces in the melting region of unfilled iPP (thin lines) and nanocomposites containing 2 wt % of SWCNTs (thick lines). The samples were heated at the indicated rates after ballistic cooling; heat flows normalized for varying heating rates.

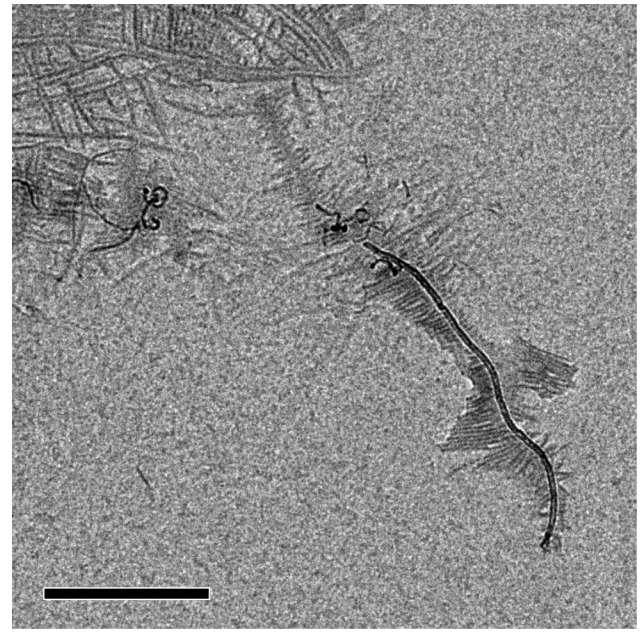

Figure 10. Bright-field TEM micrograph of an iPP/MWCNT nanocomposite ultrathin film nonisothermally crystallized from the melt at 5 °C/min; scale bar: 500 nm.

phenomenon rather than being restricted to a few specific matrix materials. For this reason, and in view of the extremely high specific surface provided by the nanofillers, the formation of an ordered crystalline interface may also be of prime technological relevance, as it was for instance recognized that the nature of the interface plays a fundamental role in the reinforce-

ment mechanism,[21,59] however without affecting the electrical conductivity of the nanocomposite.[8]

Nanocomposite Structure. The information from direct visual observation, in combination with the conclusions drawn from thermal analysis, allows us to present a structural model for the morphologies encountered in semicrystalline nanocomposites of this type. TEM imaging confirms the assumption that a transcrystalline phase is formed around the CNTs due to their strong nucleating action, whereas WAXD analysis shows that polymorphism is not involved in this morphological change. From the increase in the melting temperature it is assumed that the transcrystalline phase is of higher perfection than the more bulklike crystalline phase. The reason is probably related to the supercooling at which it was formed during the nonisothermal crystallization run, even though a higher degree of order and increased lamellar thickness have also been reported for isothermally crystallized samples.[24,31] Furthermore, this crystalline phase most likely does not undergo recrystallization upon heating due to mobility restrictions, probably resulting from a combination of polymer/filler interaction, reduced diffusion rate, and geometrical confinement, all three affecting the segmental motion required for recrystallization. Still, constant melting endset values are observed under slow heating conditions, clearly attesting the occurrence of some degree of recrystallization. The changing balance between lower and higher melting fractions therefore suggests that preferably the bulklike crystalline fraction, which is not in direct contact with the CNTs, participates in this recrystallization process. Its importance, however, progressively decreases with increasing filler loading, as more and more CNT surface becomes available for the formation of a transcrystalline interphase. Conversely, SWCNTs turn out to be significantly more effective in this respect as they provide a considerably larger surface area than MWCNTs at equal mass fraction. The amount of transcrystalline interphase material is therefore much higher in nanocomposites based on the former, and confinement effects affecting the polymer mobility are much more pronounced. In conclusion, the overall nanocomposite morphology can be regarded as a multiphase structure, in agreement with the observations from Figure 10. It consists of unaffected bulklike material, individually dispersed filler particles, and a surrounding transcrystalline interphase in which polymer chains display a reduced segmental mobility. The thickness of this interphase is probably independent of the CNT type, as it is governed only by the nature of the filler surface, which is identical in both systems.[21] Its total amount, however, scales with the external surface area of the filler and is undoubtedly much larger in SWCNT-based nanocomposites in comparison with their multi-walled counterparts.

4. Conclusions

We reported on two series of semicrystalline polypropylene nanocomposites, containing either SWCNTs or MWCNTs. A method based on latex technology was used for their preparation, allowing for the achievement of high dispersion qualities. Strong nucleating action was observed for both types of CNTs, scaling with the external surface area provided by the nanofiller. SWCNTs displayed a nucleating effect comparable to that of traditional nucleating agents. WAXD analysis of the crystalline structure did not reveal any polymorphism, showing that CNTs are exclusively α-nucleating in the quiescent crystallization conditions investigated. An increase in the melting temperature after nonisothermal crystallization pointed at a higher degree of crystalline perfection of the matrix polymer in the presence of CNTs. The complex multiple melting behavior was interpreted in terms of recrystallization phenomena occurring during heating. A detailed (MT)DSC study at varying cooling and heating rates revealed the partial suppression of crystal perfectioning as a result of a reduced polymer mobility in the vicinity of the CNTs. This effect was more pronounced in SWCNT nanocomposites due to their higher surface area. TEM imaging, for the first time, revealed the formation of a highly ordered transcrystalline morphology in iPP nanocomposites, suggesting that the high nucleating action of the CNTs restricts crystal growth to the direction perpendicular to their surface. Finally, a structure model was presented, in which the individually dispersed CNTs are separated from a weakly influenced bulklike polymer phase by a highly ordered crystalline interface with reduced mobility. The latter is potentially of high technological importance as it might account for many of the property enhancements reported for this class of nanocomposite materials.

Acknowledgment. This research is part of the research program of the Dutch Polymer Institute (Project No. 416). The work of H. Miltner was supported by a grant of the Fund for Scientific Research Flanders (FWO). The authors are grateful to M.-P. Delplancke and T. Segato (Université Libre de Bruxelles—Service de Chimie Industrielle) for WAXD analysis. H. Wautier at Solvay S.A. and M. Claes at Nanocyl S.A. are kindly acknowledged for supplying iPP latex and MWCNTs, respectively. TA Instruments is acknowledged for providing access to and assistance with the rapid-scanning DSC.

References and Notes

(1) Iijima, S. *Nature (London)* **1991**, *354*, 56–58.
(2) Ajayan, P. M.; Ebbesen, T. W. *Rep. Prog. Phys.* **1997**, *60*, 1025–1062.
(3) Thostenson, E. T.; Ren, Z. F.; Chou, T. W. *Compos. Sci. Technol.* **2001**, *61*, 1899–1912.
(4) Coleman, J. N.; Khan, U.; Gun'ko, Y. K. *Adv. Mater.* **2006**, *18*, 689–706.
(5) Coleman, J. N.; Khan, U.; Blau, W. J.; Gun'ko, Y. K. *Carbon* **2006**, *44*, 1624–1652.
(6) Gojny, F. H.; Wichmann, M. H. G.; Fiedler, B.; Kinloch, I. A.; Bauhofer, W.; Windle, A. H.; Schulte, K. *Polymer* **2006**, *47*, 2036–2045.
(7) Qunaies, Z.; Park, C.; Wise, K. E.; Siochi, E. J.; Harrison, J. S. *Compos. Sci. Technol.* **2003**, *63*, 1637–1646.
(8) Haggenmueller, R.; Guthy, C.; Lukes, J. R.; Fischer, J. E.; Winey, K. I. *Macromolecules* **2007**, *40*, 2417–2421.
(9) Bhattacharyya, A. R.; Sreekumar, T. V.; Liu, T.; Kumar, S.; Ericson, L. M.; Hauge, R. H.; Smalley, R. E. *Polymer* **2003**, *44*, 2373–2377.
(10) Assouline, E.; Lustiger, A.; Barber, A. H.; Cooper, C. A.; Klein, E.; Wachtel, E.; Wagner, H. D. *J. Polym. Sci., Part B: Polym. Phys.* **2003**, *41*, 520–527.
(11) Sandler, J. K. W.; Pegel, S.; Cadek, M.; Gojny, F. H.; van Es, M.; Lohmar, J.; Blau, W. J.; Schulte, K.; Windle, A. H.; Shaffer, M. S. P. *Polymer* **2004**, *45*, 2001–2015.
(12) Pötschke, P.; Fornes, T. D.; Paul, D. R. *Polymer* **2002**, *43*, 3247–3255.
(13) Kharchenko, S. B.; Douglas, J. F.; Obrzut, J.; Grulke, E. A.; Migler, K. B. *Nat. Mater.* **2004**, *3*, 564–568.
(14) Kim, H. M.; Kim, K.; Lee, C. Y.; Joo, J.; Cho, S. J.; Yoon, H. S.; Pejakovic, D. A.; Yoo, J. W.; Epstein, A. J. *Appl. Phys. Lett.* **2004**, *84*, 589–591.
(15) Park, C.; Ounaies, Z.; Watson, K. A.; Crooks, R. E.; Smith, J.; Lowther, S. E.; Connell, J. W.; Siochi, E. J.; Harrison, J. S.; Clair, T. L. S. *Chem. Phys. Lett.* **2002**, *364*, 303–308.
(16) Kashiwagi, T.; Grulke, E.; Hilding, J.; Harris, R.; Awad, W.; Douglas, J. *Macromol. Rapid Commun.* **2002**, *23*, 761–765.
(17) Valentini, L.; Biagiotti, J.; Kenny, J. M.; Santucci, S. *J. Appl. Polym. Sci.* **2003**, *87*, 708–713.
(18) Leelapornpisit, W.; Ton-That, M. T.; Perrin-Sarazin, F.; Cole, K. C.; Denault, J.; Simard, B. *J. Polym. Sci., Part B: Polym. Phys.* **2005**, *43*, 2445–2453.
(19) Avila-Orta, C. A.; Medellin-Rodriguez, F. J.; Davila-Rodriguez, M. V.; Aguirre-Figueroa, Y. A.; Yoon, K.; Hsiao, B. S. *J. Appl. Polym. Sci.* **2007**, *106*, 2640–2647.
(20) Grossiord, N.; Miltner, H. E.; Loos, J.; Meuldijk, J.; Van Mele, B.; Koning, C. E. *Chem. Mater.* **2007**, *19*, 3787–3792.
(21) Cadek, M.; Coleman, J. N.; Ryan, K. P.; Nicolosi, V.; Bister, G.; Fonseca, A.; Nagy, J. B.; Szostak, K.; Beguin, F.; Blau, W. J. *Nano Lett.* **2004**, *4*, 353–356.
(22) Lu, K.; Grossiord, N.; Koning, C. E.; Miltner, H. E.; Van Mele, B.; Loos, J. *Macromolecules* **2008**, 000. submitted.

(23) Grossiord, N.; Miltner, H. E.; Lu, K.; Loos, J.; Van Mele, B.; Koning, C. E.Manuscript in preparation.
(24) Quan, H.; Li, Z. M.; Yang, M. B.; Huang, R. *Compos. Sci. Technol.* **2005**, *65*, 999–1021.
(25) Varga, J.; Karger-Kocsis, J. *Polymer* **1995**, *36*, 4877–4881.
(26) Wang, C.; Liu, C. R. *Polymer* **1999**, *40*, 289–298.
(27) Brückner, S.; Meille, S. V.; Petraccone, V.; Pirozzi, B. *Prog. Polym. Sci.* **1991**, *16*, 361–404.
(28) Assouline, E.; Wachtel, E.; Grigull, S.; Lustiger, A.; Wagner, H. D.; Marom, G. *Polymer* **2001**, *42*, 6231–6237.
(29) Dasari, A.; Yu, Z. Z.; Mai, Y. W. *Macromolecules* **2007**, *40*, 123–130.
(30) Haggenmueller, R.; Fischer, J. E.; Winey, K. I. *Macromolecules* **2006**, *39*, 2964–2971.
(31) Trujillo, M.; Arnal, M. L.; Muller, A. J.; Laredo, E.; Bredeau, S.; Bonduel, D.; Dubois, P. *Macromolecules* **2007**, *40*, 6268–6276.
(32) Li, C. Y.; Li, L. Y.; Cai, W. W.; Kodjie, S. L.; Tenneti, K. K. *Adv. Mater.* **2005**, *17*, 1198–1202.
(33) Grady, B. P.; Pompeo, F.; Shambaugh, R. L.; Resasco, D. E. *J. Phys. Chem. B* **2002**, *106*, 5852–5858.
(34) Grossiord, N.; Regev, O.; Loos, J.; Meuldijk, J.; Koning, C. E. *Anal. Chem.* **2005**, *77*, 5135–5139.
(35) Grossiord, N.; Loos, J.; Meuldijk, J.; Regev, O.; Miltner, H. E.; Van Mele, B.; Koning, C. E. *Compos. Sci. Technol.* **2007**, *67*, 778–782.
(36) Danley, R. L.; Caulfield, P. A.; Aubuchon, S. R. *Am. Lab.* **2008**, *40*, 9–11.
(37) Jeon, K.; Lumata, L.; Tokumoto, T.; Steven, E.; Brooks, J.; Alamo, R. G. *Polymer* **2007**, *48*, 4751–4764.
(38) Probst, O.; Moore, E. M.; Resasco, D. E.; Grady, B. P. *Polymer* **2004**, *45*, 4437–4443.
(39) Sarno, M.; Gorrasi, G.; Sannino, D.; Sorrentino, A.; Ciambelli, P.; Vittoria, V. *Macromol. Rapid Commun.* **2004**, *25*, 1963–1967.
(40) Li, J. A.; Fang, Z. P.; Tong, L. F.; Gu, A. J.; Liu, F. *J. Polym. Sci., Part B: Polym. Phys.* **2006**, *44*, 1499–1512.
(41) Kim, Y. C.; Kim, C. Y. *Polym. Eng. Sci.* **1991**, *31*, 1009–1014.
(42) Jang, G. S.; Cho, W. J.; Ha, C. S. *J. Polym. Sci., Part B: Polym. Phys.* **2001**, *39*, 1001–1016.
(43) Varga, J. *J. Macromol. Sci.* **2002**, *41*, 1121–1171.
(44) Hoffman, J. D.; Davis, G. T., Jr. In *Treatise on Solid State Chemistry*; Hannay, N. B. Ed.; Plenum Press: New York, 1976; Vol. *3*, pp 497−614.
(45) Hoffman, J. D.; Weeks, J. J. *J. Res. Natl. Bur. Stand.* **1962**, *66A*, 13–28.
(46) Miller, R. L. In *Polymer Handbook*, 4th ed.; Brandrup,J., Immergut, E. H., Grulke, A. Eds.; John Wiley & Sons: New York, 1999.
(47) Bogoeva-Gaceva, G.; Janevski, A.; Mäder, E. *J. Adhes. Sci. Technol.* **2000**, *14*, 363–380.
(48) Schmidtke, J.; Strobl, G.; Thurn-Albrecht, T. *Macromolecules* **1997**, *30*, 5804–5821.
(49) Strobl, F. *Prog. Polym. Sci.* **2006**, *31*, 398–442.
(50) Paukkeri, R.; Lehtinen, A. *Polymer* **1993**, *34*, 4083–4088.
(51) Yadav, Y. S.; Jain, P. C. *Polymer* **1986**, *27*, 721–727.
(52) Genovese, A.; Shanks, R. A. *J. Therm. Anal. Calorim.* **2004**, *75*, 233–248.
(53) Miltner, H. E.; Rahier, H.; Pozsgay, A.; Pukanszky, B.; Van Mele, B. *Compos. Interfaces* **2005**, *12*, 787–803.
(54) Miltner, H. E.; Van Assche, G.; Pozsgay, A.; Pukanszky, B.; Van Mele, B. *Polymer* **2006**, *47*, 826–835.
(55) Miltner, H. E.; Peeterbroeck, S.; Viville, P.; Dubois, P.; Van Mele, B. *J. Polym. Sci., Part B: Polym. Phys.* **2007**, *45*, 1291–1302.
(56) Du, F. M.; Scogna, R. C.; Zhou, W.; Brand, S.; Fischer, J. E.; Winey, K. I. *Macromolecules* **2004**, *37*, 9048–9055.
(57) Fisher, F. T.; Eitan, A.; Andrews, R.; Schadler, L. S.; Brinson, L. C. *Adv. Compos. Lett.* **2004**, *13*, 105–111.
(58) Zhang, S.; Minus, M. L.; Zhu, L.; Wong, C.-P.; Kumar; S, *Polymer* **2008**, *49*, 1356–1364.
(59) Coleman, J. N.; Cadek, M.; Ryan, K. P.; Fonseca, A.; Nagy, J. B.; Blau, W. J.; Ferreira, M. S. *Polymer* **2006**, *47*, 8556–8561.

MA800643J